Gas-Phase Uranyl−Nitrile Complex Ions

Michael J. Van Stipdonk,*,† Winnie Chien,† Kellis Bulleigh,†,§ Qun Wu,† and Gary S. Groenewold‡

Department of Chemistry, Wichita State University, Wichita, Kansas 67260-0051, and Idaho National Laboratory, Idaho Falls, ID 83415-2208

Received: August 8, 2005; In Final Form: November 11, 2005

Electrospray ionization was used to generate doubly charged complex ions composed of the uranyl ion and nitrile ligands. The complexes, with general formula $[UO_2(RCN)_n]^{2+}$, $n = 0-5$ (where R═CH_3-, CH_3CH_2-, or C_6H_5-), were isolated in an ion-trap mass spectrometer to probe intrinsic reactions with H_2O. For these complexes, two general reaction pathways were observed: (a) the direct addition of one or more H_2O ligands to the doubly charged complexes and (b) charge-reduction reactions. For the latter, the reactions produced uranyl hydroxide, $[UO_2OH]$, complexes via collisions with gas-phase H_2O molecules and the elimination of protonated nitrile ligands.

Introduction

The desire to gain an understanding of intrinsic uranium cation reactivity has motivated several mass spectrometric studies, most focusing on the reactions of uranium in low oxidation states (i.e., U^+ and UO^+) with organic compounds[1−6] or oxidation of uranium ions by small molecules such as O_2, CO, N_2O, and ethylene oxide.[7−10] To improve the understanding of intrinsic uranium chemistry, particularly for higher oxidation states, we have been studying the species-dependent reactivity of a range of monopositive uranyl-ligand cations using ion-trap mass spectrometry.[11−14]

Exploration of intrinsic uranyl ion chemistry has thus far been impeded because of a lack of effective methods for generating doubly charged complexes containing UO_2^{2+}. Schwarz and co-workers[8] reported formation of the "bare" uranyl dication by gas-phase oxidation and charge exchange reactions, which yielded a value for the second ionization potential for UO_2^+ that was consistent with vertical ionization energies obtained by ab initio calculations. More recently, Gibson, Marçalo, and co-workers used laser desorption/ionization and in situ oxidation to generate gas-phase, divalent actinide dioxo cations for subsequent characterization by Fourier transform ion cyclotron resonance mass spectrometry.[15]

Gas-phase complexes containing the uranyl ion can also be generated by electrospray ionization (ESI).[11−14,16−21] For example, we have shown that ESI using solutions composed of uranyl−nitrate dissolved in a mixture of H_2O and acetone will produce doubly charged complexes in which the uranyl ion is coordinated by acetone ligands.[14] The dominant species generated featured the uranyl ion coordinated by 4 or 5 acetone ligands. However, chemical mass shift data, ion peak shapes, and a plot of fractional ion abundance vs ion desolvation temperature suggested that, in the gas phase, complexes with 5 equatorial acetone ligands are less stable than those with 4. One of our research goals is a comprehensive investigation of the influence of ligation on the intrinsic reactivity of gas-phase uranyl species. In multiple-stage (MS^n) collision-induced dissociation (CID) experiments, the doubly charged uranyl−acetone complexes did not shed their full complement of coordinating ligands but instead generated hydrated product ions (where H_2O replaced acetone ligands eliminated in the CID reactions) or charge-reduction product ions containing $[UO_2OH]^+$ or UO_2^+ coordinated by acetone and/or H_2O. At no point in the MS^n experiments were gas-phase complex ions containing the uranyl ion and two or fewer acetone or H_2O ligands observed.

In the present study ESI was used to generate gas-phase complex ions composed of the uranyl ion and acetonitrile (acn), propionitrile (pn), or benzonitrile (bzn) ligands. Unlike our earlier investigation of uranyl−acetone complex ions,[14] the use of nitrile ligands in the present case allowed the production of a series of gas-phase ions with general formula $[UO_2(RCN)_n]^{2+}$ with $n = 2-5$. For acetonitrile, the bare uranyl ion and a complex composed of the uranyl ion and a single nitrile ligand (i.e., $[UO_2(acn)_1]^{2+}$) were also produced. Generation by ESI of this group of gas-phase species allowed a direct investigation of the influence of the number and type of coordinating ligands on the intrinsic reactions of ligated uranyl ion with H_2O in the gas-phase environment of an ion trap mass spectrometer.

Experimental Section

ESI-MS, multiple-stage CID, and ion−molecule reactions were carried out using established procedures explicitly described for uranium complexation studies in refs 11−14. Uranyl nitrate hexahydrate, $UO_2(NO_3)_2{\cdot}6H_2O$ was purchased from Fluka/Sigma-Aldrich (St. Louis, MO). Acetonitrile, propionitrile, and benzonitrile (>99% purity) were purchased from Aldrich Chemical (St. Louis, MO) and used as received. A stock solution of uranyl nitrate (1 mM concentration) was prepared by dissolving the appropriate amount of solid in deionized H_2O. Spray solutions for the ESI experiment were prepared by combining portions of the $UO_2(NO_3)_2{\cdot}6H_2O$ stock solution and nitrile in a 1:100 relative molar ratio. For 1 mL total solution volume, the amount of nitrile added ranged from 5 μL for acn to 9.8 μL for bzn. These volumes of nitrile were sufficient to

* To whom correspondence should be addressed.
† Wichita State University.
‡ Idaho National Laboratory.
§ Present address: University of Kansas Medical Center, 3901 Rainbow Boulevard, Kansas City, KS 66160.

10.1021/jp054422c CCC: $33.50
Published on Web 12/17/2005

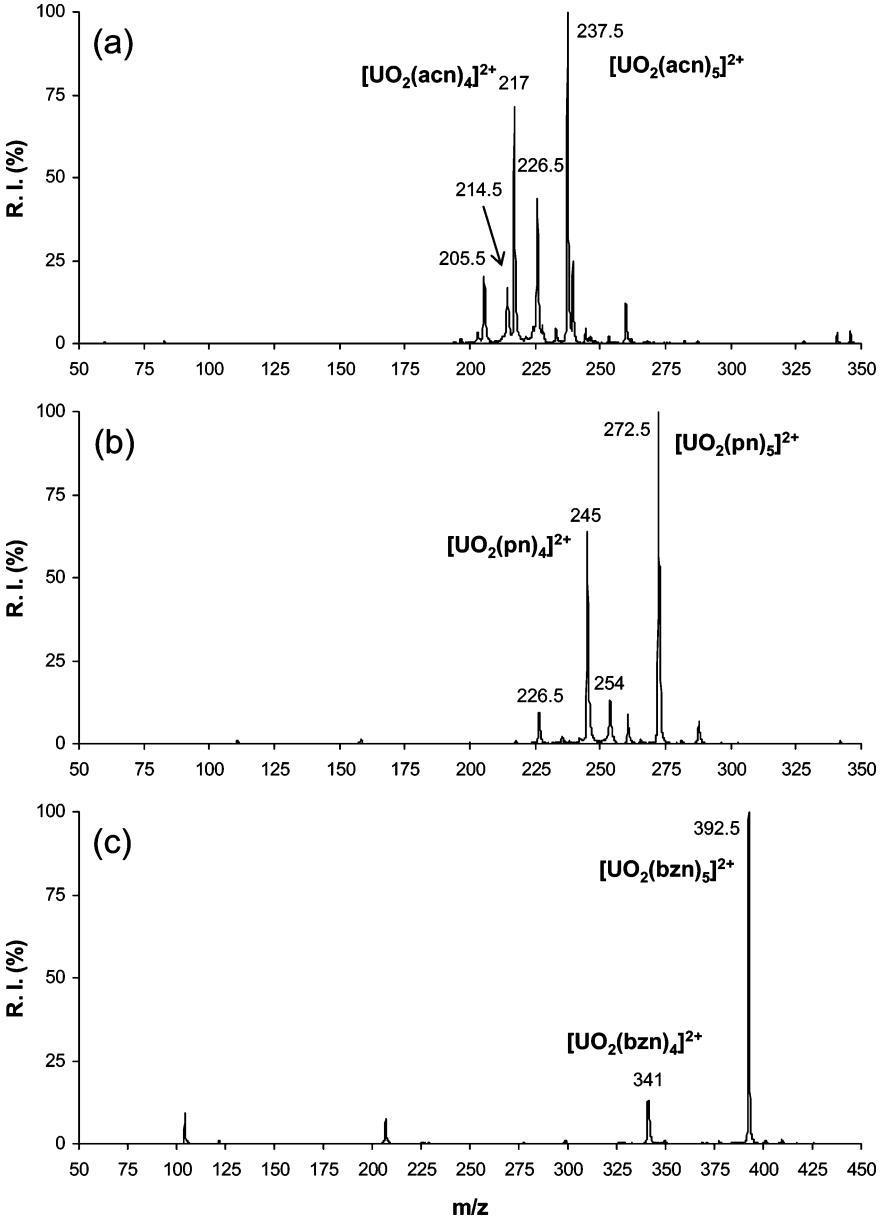

Figure 1. ESI mass spectra of solutions containing $UO_2(NO_3)2\cdot(H_2O)_6$ and (a) acetonitrile, (b) proprionitrile, and (c) benzonitrile. The uranyl ion−nitrile molar ratio was approximately 1:10 in each case.

generate abundant doubly charged uranyl−nitrile complexes but low enough to avoid the introduction of significant partial pressures of neutral nitrile into the ion trap to participate in ion−molecule reactions.

ESI mass spectra were collected using a Finnigan LCQ-Deca ion-trap mass spectrometer (ThermoFinnigan Corporation, San Jose, CA). The spray solutions were infused into the ESI-MS instrument using the incorporated syringe pump at a flow rate of 3−5 μL/min. The atmospheric pressure ionization stack settings for the LCQ (lens voltages, quadrupole, and octapole voltage offsets, etc.) were optimized for maximum ion transmission to the ion-trap mass analyzer by using the autotune routine within the LCQ Tune program. The spray needle voltage was maintained at +5 kV and the N_2 sheath gas flow at 25 units (approximately 0.375 Ls/minute). For most experiments, the heated capillary, used for ion desolvation prior to injection into the ion trap, was maintained at 120 °C to maximize both the total ion signal and the production of doubly charged complexes. Helium was used as the bath/buffer gas to improve trapping efficiency and as the collision gas for CID experiments. Ion charge states were confirmed by examining the isotopic peak spacing using the ZoomScan, high-resolution function of the LCQ-Deca. Doubly charged species were identified by isotopic (primarily ^{12}C and ^{13}C from the nitrile ligands) peak spacing of 0.5 mass units (u).

To probe gas-phase ligand-addition and charge-exchange reactions, the doubly charged uranyl−acn complex ions were isolated individually, stored within the ion trap, and allowed to react with H_2O within the He bath gas. Isolation widths of 0.7−1.2 mass units were centered on the *m*/*z* value of the precursor ion. The isolation width for a given uranyl complex was chosen empirically to provide an optimal compromise between abundant ion signal and the isolation of single isotopic precursor ion peaks. For the isolation/reaction studies, the activation amplitude (arbitrary to the LCQ system, represents a percentage of 5 V, normalized for precursor ion mass) was set at 0 V. The activation *Q* (used to adjust the q_z value for the resonant excitation of the precursor ion during the CID experiment) was set at 0.3. After the isolation period, the precursor and product ions were scanned out of the trap and detected as part of the automated mass

TABLE 1: Uranyl Complexes Generated by ESI of $UO_2(NO_3)_2 \cdot (H_2O)_6$ in Water/Nitrile Solution

m/*z* ratio	composition assignment
	Acetonitrile
135	UO_2^{2+}
155.5	$[UO_2(acn)_1]^{2+}$
176	$[UO_2(acn)_2]^{2+}$
185	$[UO_2(acn)_2(H_2O)_1]^{2+}$
194	$[UO_2(acn)_2(H_2O)_2]^{2+}$
196.5	$[UO_2(acn)_3]^{2+}$
203	$[UO_2(acn)_2(H_2O)_3]^{2+}$
205.5	$[UO_2(acn)_3(H_2O)_1]^{2+}$
214.5	$[UO_2(acn)_3(H_2O)_2]^{2+}$
217	$[UO_2(acn)_4]^{2+}$
226	$[UO_2(acn)_4(H_2O)_1]^{2+}$
237.5	$[UO_2(acn)_5]^{2+}$
	Propionitrile
190	$[UO_2(pn)_2]^{2+}$
199	$[UO_2(pn)_2(H_2O)_1]^{2+}$
208	$[UO_2(pn)_2(H_2O)_2]^{2+}$
217	$[UO_2(pn)_2(H_2O)_3]^{2+}$
217.5	$[UO_2(pn)_3]^{2+}$
226.5	$[UO_2(pn)_3(H_2O)_1]^{2+}$
235.5	$[UO_2(pn)_3(H_2O)_2]^{2+}$
245	$[UO_2(pn)_4]^{2+}$
254	$[UO_2(pn)_4(H_2O)_1]^{2+}$
272.5	$[UO_2(pn)_5]^{2+}$
	Benzonitrile
238	$[UO_2(bzn)_2]^{2+}$
289.5	$[UO_2(bzn)_3]^{2+}$
298.5	$[UO_2(bzn)_3(H_2O)_1]^{2+}$
341	$[UO_2(bzn)_4]^{2+}$
392.5	$[UO_2(bzn)_5]^{2+}$

analysis operation. Direct comparisons of complex reactivity were carried out using 30-ms isolation times. The pressure within the vacuum system was ca. 1.2×10^{-5} Torr during experimental trials. H_2O is present as an indigenous species in the vacuum system and is admitted into the vacuum system directly because of its use in the spray solvent mixture. It is estimated that the partial pressures of H_2O were ca. 1×10^{-6} Torr based on previous hydration studies using similar operating parameters.[13,22] Because ESI is an atmospheric pressure ionization method, N_2 and O_2 from the ambient environment were likely present within the He bath gas. N_2 is also admitted into the ion trap because of its use as the ESI sheath gas. The ultimate goal of this study was to determine the influence of the number and type of nitrile ligands on the uranyl complex reactions with H_2O rather than a rigorous evaluation of gas-phase reaction rate constants. The latter would require accurate measurements of neutral reagent partial pressures, either by calibrated ion gauge measurements or use of standard ion−molecule reactions that involve the reagents employed here.

For CID (MS/MS and MS^n), ion isolation parameters used were similar to those used for the ion storage/reactivity studies, except that collisional activation was carried out using activation amplitudes of 10−20%. These activation amplitudes range from approximately 0.4−0.7 V in the laboratory frame of reference. Applied collision voltages of this magnitude were sufficient to reduce the precursor ion intensity to ∼10% relative abundance.

Results and Discussion

ESI Mass Spectra. Figure 1 shows ESI mass spectra generated from spray solutions containing $[UO_2(NO_3)_2 \cdot (H_2O)_6]$ and acetonitrile (Figure 1a), propionitrile (Figure 1b), or benzonitrile (Figure 1c) in a 1:100 relative molar ratio. A summary of the ion species (*m*/*z* ratios and proposed composition) observed in the three spectra is provided in Table 1. Proposed compositions were confirmed using multiple-stage CID. As in our earlier study of doubly charged complex ions generated from water−acetone mixtures,[14] we found that the general distribution of ions in the ESI spectrum was influenced by the temperature of the heated capillary used in the LCQ-Deca to desolvate ions prior to their transmission to the ion trap mass spectrometer. The best compromise between high overall ion signal and maximum production of doubly charged species was found at desolvation capillary temperatures between 100 and 120 °C. The spectra shown in Figure 1 were collected at 120°C.

For each nitrile used in this study, the principal doubly charged uranyl−nitrile complex ions generated were $[UO_2(RCN)_4]^{2+}$ and $[UO_2(RCN)_5]^{2+}$. Abundant doubly charged complexes composed of uranyl ion with a mix of acn and H_2O ligands were also observed. As is apparent in Figure 1, the intensities of analogous peaks were significantly lower when pn was used as the nitrile ligand and were not discernible above background when bzn was used instead. The decrease in abundance of complexes containing H_2O ligands scaled with the increase in nitrile basicity and likely reflected changes in the competition between nitrile and H_2O ligands for equatorial binding sites of the uranyl ion in solution and during the ion-desolvation steps (on the LCQ platform, desolvation is affected both by an N_2 sheath gas and the heated capillary) prior to introduction of ions into the ion trap.

In general, weaker binding of H_2O ligands relative to nitrile ligands, particularly for the uranyl−acetonitrile system, was apparent in an examination of the peak shapes and *m*/*z* values measured for the mixed ligand complexes (data not shown). Those ions containing H_2O ligands featured pronounced tails to the low-mass side, and significant chemical mass shifts[23,24] (∼0.1 mass unit). Previous work has established that the peak tailing and mass shifts for gas-phase complex ions are due to ion instability and decomposition during analytical scans in the ion trap.[25,26] Our previous work with uranyl−acetone complexes demonstrated that the peak tails and chemical mass shifts increased with increasing coordination number, and reflected differences in complex ion stability.[14]

Isolation of $[UO_2(acn)_n]^{2+}$, $n = 0-5$. Mass spectra generated by the isolation of $[UO_2(acn)_n]^{2+}$, n = 0−5, in the ion-trap mass spectrometer (isolation/storage time of 30 ms) are shown in Figure 2. It is important to note that, in the isolation step, all ions except for the precursor ion of interest were resonantly ejected from the ion trap. Composition assignments for the precursor and product ion species shown in Figure 2 and their relative intensities are listed in Table 2. In general, two reaction pathways were observed: (a) the direct addition of one or more H_2O ligands to the doubly charged precursor ions and (b) charge reduction reactions that generated singly charged complex ions containing $[UO_2OH]^+$.

As shown in Figure 2a, isolation of UO_2^{2+} at *m*/*z* 135 resulted in the formation of UO_2^+ at *m*/*z* 270 and $[UO_2OH]^+$ at *m*/*z* 287. CID (formally MS^3) of the peak at *m*/*z* 287 produced UO_2^+ at *m*/*z* 270 via the elimination of 17 mass units (u), consistent with the proposed hydroxide composition. In addition, creation of the hydroxide was confirmed through a comparison of the intrinsic hydration rates of the species at *m*/*z* 287 to earlier investigation of the hydration of $[UO_2OH]^+$ derived from solutions of uranyl nitrate in pure water[13] (data not shown). The peak at *m*/*z* 135 was <1% relative abundance in the ESI mass spectrum, and contributions of ^{18}O and ^{235}U to the isotopic distribution of the presumed UO_2^{2+} ion are minor. These two factors combined to make identification of the charge state for

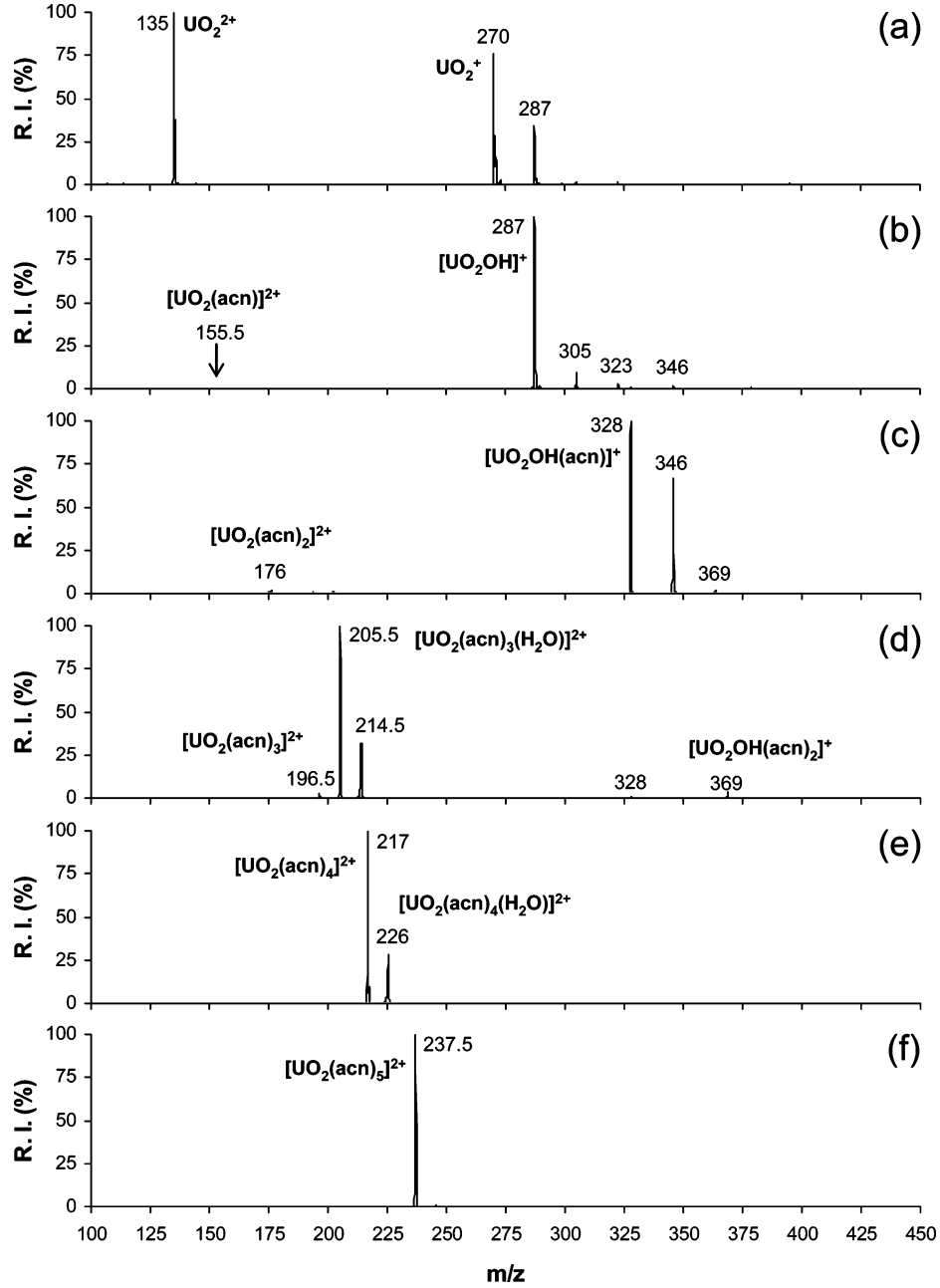

Figure 2. Product ion spectra generated by the isolation and storage of doubly charged uranyl−acetonitrile complex ions in a quadrupole ion trap for 30 ms. (a) UO_2^{2+}, (b) $[UO_2(acn)_1]^{2+}$, (c) $[UO_2(acn)_2]^{2+}$, (d) $[UO_2(acn)_3]^{2+}$, (e) $[UO_2(acn)_4]^{2+}$, and (f) $[UO_2(acn)_5]^{2+}$.

the species at *m*/ *z* 135 by a high-resolution scan impossible. However, the appearance of product ions at *m*/*z* 270 and 287, and identification of the latter as $[UO_2OH]^+$, strongly supports the composition assignment for *m*/*z* 135 as UO_2^{2+}.

A decrease in the UO_2^{2+} peak intensity, and rise in UO_2^+ and $[UO_2OH]^+$ peak intensities, were observed for isolation times extending to 1 s (data not shown). H_2O adducts to both UO_2^+ and $[UO_2OH]^+$ were also observed at longer isolation/storage times. At no point, however, was direct H_2O ligand addition to UO_2^{2+} competitive with the charge reduction pathways (formation of UO_2^+ and $[UO_2OH]^+$). Experimentally determined ionization energies in the range of 14−15 eV have been reported for monopositive dioxouranium cation, UO_2^+.[8,15] This range is significantly higher than the ionization energies of H_2O, acn, or O_2 (ca. 12.6, 12.2, and 12.1 eV, respectively[27]), suggesting that electron transfer, when observed, could arise from collisions between any of these neutral molecular species and UO_2^{2+} in the gas-phase environment of the ion trap. The charge reduction process involving formation of uranyl−hydroxide species implicates collisions with gas-phase H_2O.

Isolation of $[UO_2(acn)_1]^{2+}$ at *m*/*z* 155.5 (Figure 2b) lead nearly exclusively to the charge-exchange product $[UO_2OH]^+$ at *m*/*z* 287. At extended isolation times (100−1000 ms, data not shown), peaks at *m*/*z* 305, 323, and 341, created by H_2O addition to $[UO_2OH]^+$, were also observed. The formation of the hydroxide would presumably proceed through reaction 1, which would involve a reactive collision with an H_2O molecule, transfer of a proton to the acetonitrile ligand, transfer of OH^- to the uranyl ion, and coulomb explosion to separate the charged products

$$[UO_2(acn)_1]^{2+} + H_2O \rightarrow [UO_2(acn)_1(H_2O)]^{2+}* \leftrightarrow [UO_2OH(acnH)]^{2+}* \rightarrow [UO_2OH]^+ + (acn)H^+ \quad (1)$$

The default (normal range) scan waveform of the LCQ imposes a low-mass cutoff in the tandem mass spectrometry

TABLE 2: Product Ion *m/z* Values and Composition Assignments for Isolation of $[UO_2(acn)_n]^{2+}$, $n = 0-5$, and Exposure to Gas-Phase H_2O

	ligand addition products		charge-exchange products	
precursor	*m/z* (rel int. %)	composition	*m/z* (rel int. %)	composition
UO_2^{2+}			270 (76)	UO_2^+
			287 (43)	$[UO_2OH]^+$
			305 (2)	$[UO_2OH(H_2O)_1]^+$
			323 (2)	$[UO_2OH(H_2O)_2]^+$
$[UO_2(acn)_1]^{2+}$			287 (100)	$[UO_2OH]^+$
			305 (10)	$[UO_2OH(H_2O)_1]^+$
			323 (2.5)	$[UO_2OH(H_2O)_2]^+$
			328 (1.5)	$[UO_2OH(acn)_1]^+$
			346 (1.2)	$[UO_2OH(acn)_1(H_2O)]^+$
$[UO_2(acn)_2]^{2+}$	185 (0.1)	$[UO_2(acn)_2(H_2O)_1]^{2+}$	328 (100)	$[UO_2OH(acn)_1]^+$
	194 (0.6)	$[UO_2(acn)_2(H_2O)_2]^{2+}$	346 (70)	$[UO_2OH(acn)_1(H_2O)]^+$
	203 (3)	$[UO_2(acn)_2(H_2O)_3]^{2+}$	369 (5)	$[UO_2OH(acn)_2]^+$
$[UO_2(acn)_3]^{2+}$	205.5 (100)	$[UO_2(acn)_3(H_2O)_1]^{2+}$	328 (0.5)	$[UO_2OH(acn)_1]^+$
	214.5 (32)	$[UO_2(acn)_3(H_2O)_2]^{2+}$	369 (8)	$[UO_2OH(acn)_2]^+$
$[UO_2(acn)_4]^{2+}$	226 (30)	$[UO_2(acn)_4(H_2O)_1]^{2+}$		
$[UO_2(acn)_5]^{2+}$				

TABLE 3: Product Ion *m/z* Values and Composition Assignments for Isolation of $[UO_2(pn)_n]^{2+}$, $n = 2-5$, and Exposure to Gas-Phase H_2O

	ligand addition products		charge-exchange products	
precursor	*m/z* (rel int. %)	composition	*m/z* (rel int. %)	composition
$[UO_2(pn)_2]^{2+}$	199 (2)	$[UO_2(pn)_2(H_2O)_1]^{2+}$	56 (33)	$(acn+H)^+$
	208 (32)	$[UO_2(pn)_2(H_2O)_2]^{2+}$	342 (30)	$[UO_2OH(pn)_1]^+$
	217 (37)	$[UO_2(pn)_2(H_2O)_3]^{2+}$	360 (100)	$[UO_2OH(pn)_1(H_2O)]^+$
			378 (3)	$[UO_2OH(pn)_1(H_2O)_2]^+$
$[UO_2(pn)_3]^{2+}$	226.5 (100)	$[UO_2(pn)_3(H_2O)_1]^{2+}$	56 (0.5)	$(acn+H)^+$
	235.5 (32)	$[UO_2(pn)_3(H_2O)_2]^{2+}$	342 (0.3)	$[UO_2OH(pn)_1]^+$
			397 (1)	$[UO_2OH(pn)_2]^+$
$[UO_2(pn)_4]^{2+}$	254 (21)	$[UO_2(pn)_4(H_2O)_1]^{2+}$		
$[UO_2(pn)_5]^{2+}$				

TABLE 4: Product Ion *m/z* Values and Composition Assignments for Isolation of $[UO_2(bzn)_n]^{2+}$, $n = 2-5$, and Exposure to Gas-Phase H_2O

	ligand addition products		charge-exchange products	
precursor	*m/z* (rel int. %)	composition	*m/z* (rel int. %)	composition
$[UO_2(bzn)_2]^{2+}$	247 (2)	$[UO_2(bzn)_2(H_2O)_1]^{2+}$	104 (1)	$(bzn+H)^+$
	256 (100)	$[UO_2(bzn)_2(H_2O)_2]^{2+}$	390 (2)	$[UO_2OH(bzn)_1]^+$
	265 (62)	$[UO_2(bzn)_2(H_2O)_3]^{2+}$	408 (7)	$[UO_2OH(bzn)_1(H_2O)]^+$
			426 (0.3)	$[UO_2OH(bzn)_1(H_2O)_2]^+$
$[UO_2(bzn)_3]^{2+}$	298.5 (14)	$[UO_2(bzn)_3(H_2O)_1]^{2+}$		
$[UO_2(bzn)_4]^{2+}$	350 (3)	$[UO_2(bzn)_4(H_2O)_1]^{2+}$		
$[UO_2(bzn)_5]^{2+}$				

mode at *m/z* 50, prohibiting the observation of both charged products in reaction 1 within the product ion spectrum. Figure 3a shows the product ion spectrum generated when the *m/z* 155.5 precursor ion was isolated and stored in the ion trap using a low-mass waveform, which permits collection of mass spectra over the limited *m/z* range of 15−200. The only product ion observed in Figure 3a appeared at *m/z* 42, the *m/z* ratio expected for protonated acn.

Figure 2c shows the spectrum that resulted from the isolation of the $[UO_2(acn)_2]^{2+}$ complex ion at *m/z* 176. Adduct peaks corresponding to the direct addition of 1, 2, and 3 H_2O ligands to the doubly charged species were observed at *m/z* 185, 194, and 203, respectively. The charge-reduction pathway was dominant for $[UO_2(acn)_2]^{2+}$, leading to the formation of $[UO_2OH(acn)]^+$ at *m/z* 328, a hydrated version of the species at *m/z* 346 and a minor peak at *m/z* 369, $[UO_2OH(acn)_2]^+$. Figure 3b shows the product ion spectrum generated when $[UO_2(acn)_2]^{2+}$ was isolated using the low-mass waveform, and the appearance of protonated acn at *m/z* 42 suggests that formation of the peak at *m/z* 328 occurs via a pathway similar the one proposed in reaction 1. CID of the peak at *m/z* 328 (formally MS^3) produced $[UO_2OH]^+$ at *m/z* 287 via elimination of 41 u, consistent with

TABLE 5: Product Ion M/z Values and Composition Assignments for CID of $[UO_2(acn)_n]^{2+}$, $n = 1-5$

	CID products	
precursor	*m/z* (rel int. %)	composition
$[UO_2(acn)_1]^{2+}$	287 (100)	$[UO_2OH]^+$
	305 (6)	$[UO_2OH(H_2O)_1]^+$
	323 (0.6)	$[UO_2OH(H_2O)_2]^+$
	328 (3)	$[UO_2OH(acn)_1]^+$
	346 (1.2)	$[UO_2OH(acn)_1(H_2O)_1]^+$
$[UO_2(acn)_2]^{2+}$	287 (8.5)	$[UO_2OH]^+$
	328 (100)	$[UO_2OH(acn)_1]^+$
	346 (76)	$[UO_2OH(acn)_1(H_2O)]^+$
	364 (0.6)	$[UO_2OH(acn)_1(H_2O)_2]^+$
$[UO_2(acn)_3]^{2+}$	176 (2)	$[UO_2(acn)_2]^{2+}$
	328 (50)	$[UO_2OH(acn)_1]^+$
	346 (26)	$[UO_2OH(acn)_1(H_2O)_1]^+$
	369 (5)	$UO_2OH(acn)_2]^+$
$[UO_2(acn)_4]^{2+}$	196.5 (4)	$[UO_2(acn)_3]^{2+}$
	205.5 (50)	$[UO_2(acn)_3(H_2O)]^{2+}$
	214.5 (17)	$[UO_2(acn)_3(H_2O)_2]^{2+}$
	287 (1)	$[UO_2OH]^+$
	369 (5)	$UO_2OH(acn)_2]^+$
$[UO_2(acn)_5]^{2+}$	217 (100)	$[UO_2(acn)_4]^{2+}$
	226 (26)	$[UO_2(acn)_4(H_2O)]^{2+}$

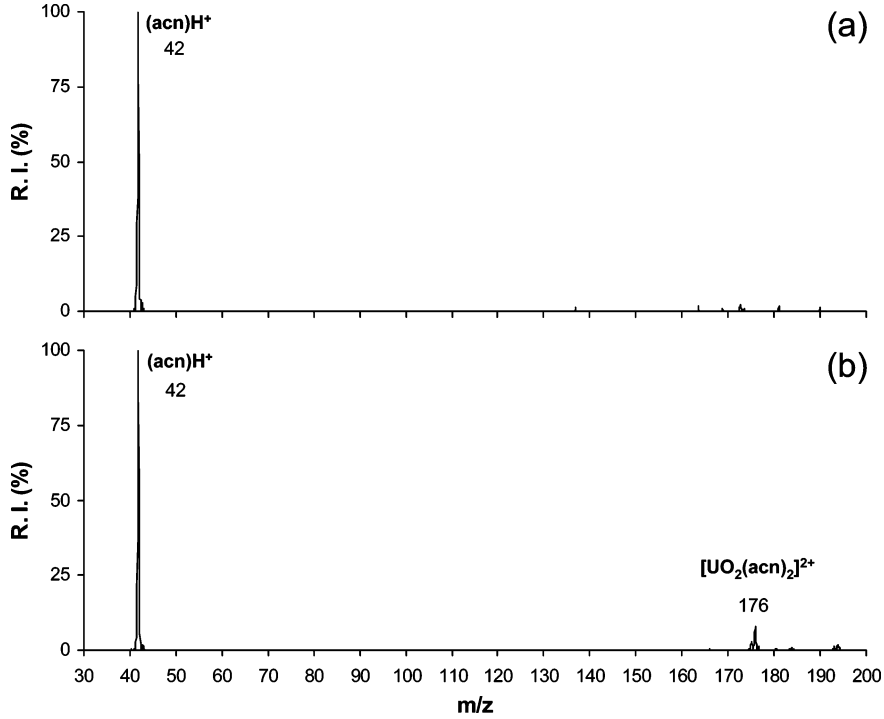

Figure 3. Product ion spectra generated by the isolation of doubly charged uranyl−acetonitrile complex ions. (a) $[UO_2(acn)_1]^{2+}$ and (b) $[UO_2(acn)_2]^{2+}$. Spectra were collected using the low mass waveform, which allows collection of spectra in the limited *m*/*z* range of 25−200.

the presence of a single acn ligand within the precursor ion. Two pathways were observed for the CID of the peak at *m*/*z* 346 (formally MS^3): loss of 18 u (H_2O) to produce the species at *m*/*z* 328 and loss of 59 (H_2O and acn) to produce *m*/ *z* 287.

The relative intensity of the species at 346 in Figure 2c was similar to the intensity for the same species in a separate experiment in which the *m*/*z* 328 product ion (generated by isolation and storage of the doubly charged species at *m*/*z* 176) was subsequently isolated and stored in the ion trap for 30 ms. This observation suggests that the species at *m*/*z* 346 observed in Figure 2c is the result of H_2O addition to the *m*/*z* 328 product derived from the isolation of $[UO_2(acn)_2]^{2+}$]. The minor product ion at *m*/*z* 369, however, was more abundant in the spectrum shown in Figure 2c than when the species at *m*/*z* 328 was independently isolated and stored, suggesting that the formation of this ion does not involve the addition of acn to $[UO_2OH(acn)]^+$ by an ion−molecule reaction (consistent with the low partial pressure of acn in the ion trap expected due to the small volume of the nitrile added to the spray solvent). The peak at *m*/*z* 369 may instead have been formed by direct hydroxide transfer to $[UO_2(acn)_2]^{2+}$ via the reaction

$$[UO_2(acn)_2]^{2+} + 2H_2O \rightarrow [UO_2(acn)_2(H_2O)_2]^{2+*} \leftrightarrow$$
$$[UO_2OH(acn)_2H_3O]^{2+*} \rightarrow [UO_2OH(acn)_2]^{+} + H_3O^{+} \quad (2)$$

With extended isolation times (100−1000 ms, data not shown), the $[UO_2OH(acn)(H_2O)]^+$ species at *m*/*z* 346 became the base peak, and a dihydrate species, $[UO_2OH(acn)(H_2O)_2]^+$, at *m*/*z* 364 also appeared.

For the isolation and storage of $[UO_2(acn)_3]^{2+}$and $[UO_2(acn)_4]^{2+}$ (parts d and e of Figure 2, respectively), ligand addition reactions dominated the charge reduction processes. Isolation of $[UO_2(acn)_3]^{2+}$ at *m*/*z* 196.5 generated mono- and dihyrdate versions, i.e., $[UO_2(acn)_3(H_2O)]^{2+}$ and $[UO_2(acn)_3(H_2O)_2]^{2+}$, of the complex at *m*/*z* 205.5 and 214.5, respectively. The charge-reduction products observed for the isolation of $[UO_2(acn)_3]^{2+}$ included $[UO_2OH(acn)]^+$ and $[UO_2OH(acn)_2]^+$. Isolation of $[UO_2(acn)_4]^{2+}$ led to the addition of a single H_2O or acn ligand, and no charge-reduction product ions were observed. With extended isolation times (data not shown), the $[UO_2(acn)_3]^{2+}$ and $[UO_2(acn)_4]^{2+}$ complexes added 2 and 1 H_2O molecules, respectively, to furnish ions with 5 total equatorial ligands. As shown in Figure 2f, isolation of $[UO_2(acn)_5]^{2+}$ produced no adduct species or charge reduction products. The absence of ligand addition reactions is generally consistent with a preferred equatorial coordination number of 5 for the uranyl ion in condensed-phase studies,[28−31] theoretical calculations,[32] and with previous studies of intrinsic ligand addition reactions for singly charged gas-phase uranyl nitrate and acetate complex ions[13] and doubly charged uranyl−acetone complexes.[14]

Isolation of $[UO_2(pn)_n]^{2+}$, $n = 2-5$. Mass spectra generated by the isolation of $[UO_2(pn)_n]^{2+}$, n = 2−5, in the ion-trap mass spectrometer are shown in Figure 4. For pn, isolation of the bare uranyl ion or $[UO_2(pn)_1]^{2+}$ was not possible. We attribute this to a higher intrinsic hydration tendency for the pn complexes relative to the acn complexes, due to the increased number of vibrational degrees of freedom with the larger ligand. A larger number of oscillators may accommodate better reaction exothermicity and thus stabilize adducts as they are formed in association reactions. A similar effect was recently reported for the intrinsic hydration of Ag^+−alcohol complexes[33] and for uranyl−acetone complex cations.[14] A hydrated form of the complex, $[UO_2(pn)_1(H_2O)_1]^{2+}$, was produced by ESI. Attempts to dissociate this ion to generate the $[UO_2(pn)_1]^{2+}$ species were complicated by a rapid hydration reaction that re-formed $[UO_2(pn)_1(H_2O)_1]^{2+}$.

The formation of mono-, di-, and trihydrates at *m*/*z* 199, 208, and 217, respectively, was observed following isolation of $[UO_2(pn)_2]^{2+}$ at *m*/*z* 190 (Figure 3a). The abundances of H_2O adducts to the pn complex were significantly higher than those generated by isolation of the analogous acn complex for an equivalent period of time (Figure 4c), consistent with the positive influence of an increased number of vibrational degrees of freedom to accommodate reaction exothermicity.

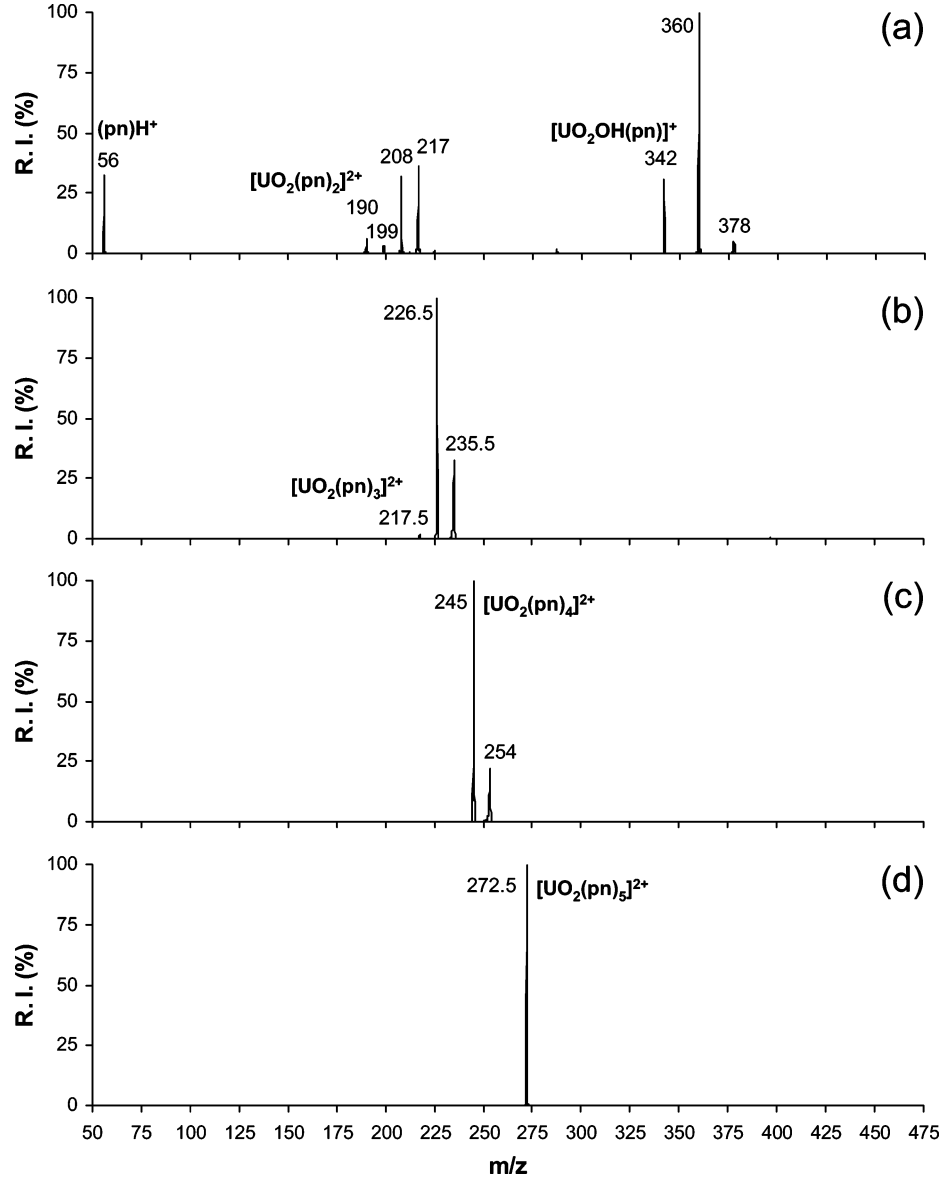

Figure 4. Product ion spectra generated by the isolation and storage of doubly charged uranyl−propionitrile complex ions in a quadrupole ion trap for 30 ms. (a) $[UO_2(pn)_2]^{2+}$, (b) $[UO_2(pn)_3]^{2+}$, (c) $[UO_2(pn)_4]^{2+}$, and (d) $[UO_2(pn)_5]^{2+}$.

As for the analogous acn complex, the dominant charge reduction reaction pathway observed for $[UO_2(pn)_2]^{2+}$ was formation of $[UO_2OH(pn)]^+$ at *m*/*z* 342 and a hydrated version of the species at *m*/*z* 360. The presence of pn and H_2O ligands was confirmed by loss of 55 u from the species at *m*/*z* 342 and of 18 and 73 u from the species at *m*/*z* 360 in subsequent CID steps (formal MS^3). The relative intensity of the species at 360 was similar to the intensity for the same species in a separate experiment in which the *m*/*z* 360 product ion (generated by isolation and storage of the doubly charged species at *m*/*z* 190) was subsequently isolated and stored in the ion trap for 30 ms, suggesting that the species at *m*/*z* 360 observed in Figure 4a is the result of H_2O addition to the *m*/*z* 342 product derived from the isolation of $[UO_2(pn)_2]^{2+}$. An important feature of the spectrum in Figure 4a is the appearance of a peak at *m*/*z* 56, consistent with the formation of protonated pn. The appearance of this peak further supports the formation of the uranyl−hydroxide product via a process that involved interactions with an H_2O collision partner, transfer of proton to a nitrile ligand, retention of the hydroxide ion, and then fission of the activated complex as proposed in reaction 1.

Only direct ligand addition reactions were observed for the isolation and storage of $[UO_2(pn)_3]^{2+}$ and $[UO_2(pn)_4]^{2+}$ (parts b and c of Figure 4, respectively). The $[UO_2(pn)_3]^{2+}$ complex at *m*/*z* 217.5 generated mono and dihyrdates, $[UO_2(pn)_3(H_2O)]^{2+}$ and $[UO_2(pn)_3(H_2O)_2]^{2+}$, at *m*/*z* 226.5 and 235.5, respectively. The $[UO_2(pn)_4]^{2+}$ complex at *m*/*z* 245 added a single H_2O molecule to make the monohydrate at *m*/*z* 254. As with the acn version of the complex, no ligand addition was observed following the isolation of the $[UO_2(pn)_5]^{2+}$ complex at *m*/*z* 272.5. At extended isolation times (100−1000 ms, data not shown), the $[UO_2(pn)_3]^{2+}$and $[UO_2(pn)_4]^{2+}$ complexes added to 2 and 1 H_2O molecules, respectively, to furnish ions with 5 total equatorial ligands. A preliminary investigation of the hydration rates for the pn complexes suggest that the rates for H_2O addition are lower than for the acn complexes. A comprehensive investigation of ligand addition rates to the complexes, including kinetic modeling, is currently being conducted and will be reported at a later date.

Isolation of $[UO_2(bzn)_n]^{2+}$, $n = 2-5$. Mass spectra generated by the isolation of $[UO_2(bzn)_n]^{2+}$, $n = 2-5$, are shown in Figure 5. As with pn, isolation of the bare uranyl ion or $[UO_2(bzn)_1]^{2+}$

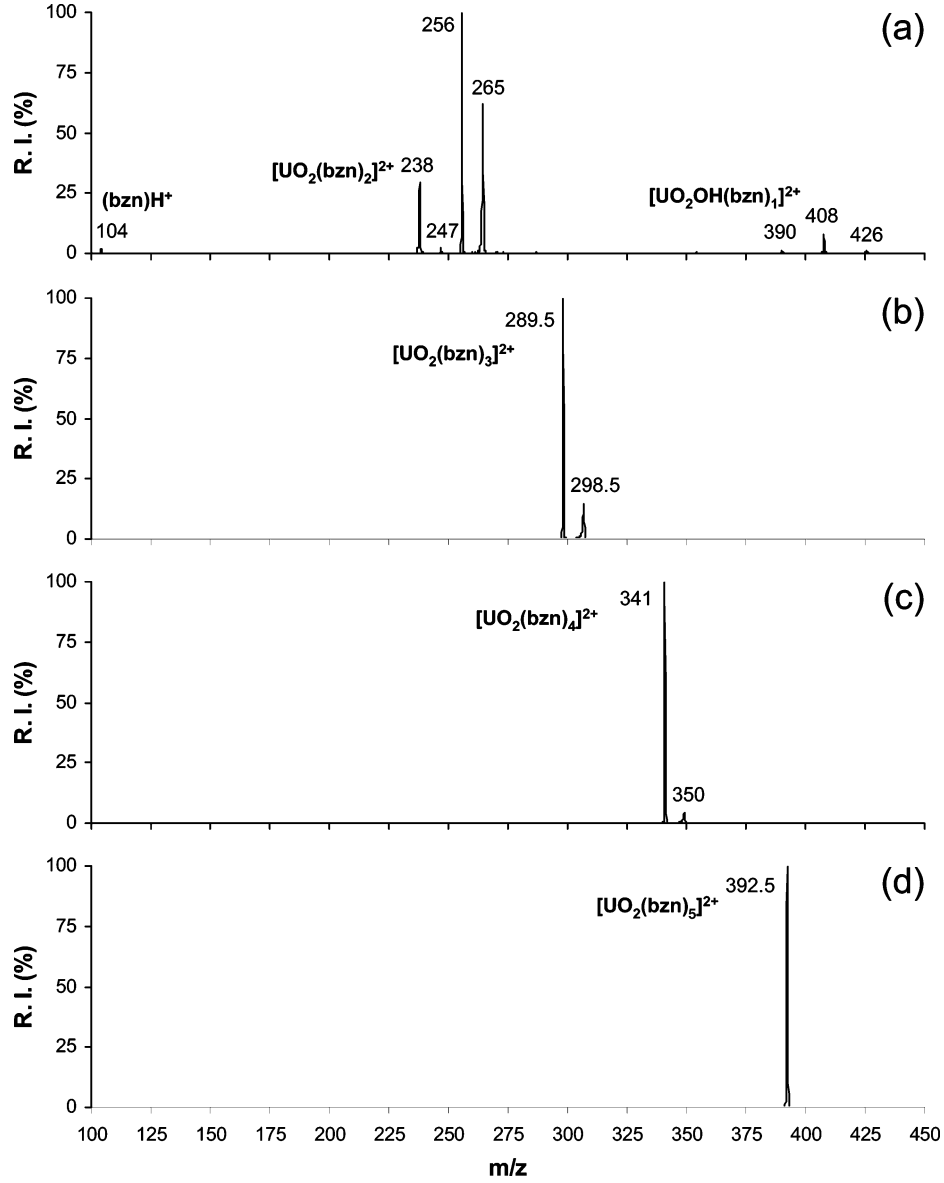

Figure 5. Product ion spectra generated by the isolation and storage of doubly charged uranyl−benzonitrile complex ions in a quadrupole ion trap for 30 ms. (a) $[UO_2(bzn)_2]^{2+}$, (b) $[UO_2(acn)_3]^{2+}$, (c) $[UO_2(bzn)_4]^{2+}$, and (d) $[UO_2(bzn)_5]^{2+}$.

was not possible. Unlike the results observed for the acn and pn complexes, the dominant products generated by isolation of $[UO_2(bzn)_2]^{2+}$ at *m*/*z* 238 (Figure 4a) were those formed by direction ligand addition (formation of mono-, di-, and trihydrates at *m*/*z* 247, 256, and 265, respectively) rather than charge reduction. The intensities of these adducts were significantly higher that those generated from the isolation of the analogous pn and acn complex, which further supports the proposal that accommodation of reaction exothermicity by internal modes in the species with larger, more complex ligands enhances the potential for direct ligand addition. Though the charge-exchange products for the bzn complexes were of overall lower abundance, the species generated were analogous to those observed for the pn and acn complexes, namely, $[UO_2OH(bzn)]^+$, $[UO_2OH(bzn)(H_2O)]^+$, and $[UO_2OH(bzn)(H_2O)_2]^+$ at *m*/*z* 390, 408, and 426, respectively. Composition assignments were confirmed through the observation of the elimination of bzn or bzn and H_2O in subsequent CID steps (formally MS^3).

For the isolation and storage of $[UO_2(bzn)_3]^{2+}$ (*m*/*z* 289.5) and $[UO_2(bzn)_4]^{2+}$ (*m*/*z* 341), shown in parts b and c of Figure 5, only ligand addition reactions were observed, producing H_2O adducts at *m*/*z* 298.5 and 350, respectively. Isolation of $[UO_2(bzn)_4]^{2+}$ led to the addition of a single H_2O, and $[UO_2(bzn)_5]^{2+}$ (Figure 5d) was unreactive. At extended isolation times, the intensity of the hydrate peaks increased more slowly than for the pn and acn versions of the complexes, and the addition of a second H_2O ligand to $[UO_2(bzn)_3]^{2+}$ was not favored. While further comment on the intrinsic hydration rates will be made at a later date, the decrease in apparent hydration tendency from acn to pn to bzn versions of $[UO_2(RCN)_3]^{2+}$ and $[UO_2(RCN)_4]^{2+}$ is likely attributable to a combination of increasing ligand basicity (bzn > pn > acn), and thus greater donation of charge to the uranyl ion, and to potential steric effects about the equatorial coordination sites.

Intrinsic Reactivity with H_2O. In general, the tendency for direct H_2O ligand addition to the uranyl−nitrile complexes is influenced by the number of nitrile ligands in the precursor uranyl complex and their complexity. For example, H_2O addition was not observed for UO_2^{2+} and $[UO_2(acn)_1]^{2+}$, was observed to a small extent for $[UO_2(acn)_2]^{2+}$, and became dominant for $[UO_2(acn)_3]^{2+}$ and $[UO_2(acn)_4]^{2+}$. With respect to the nitrile ligand, the tendency for direct H_2O addition to precursor ions with 2 nitrile ligands increased with a trend acn < pn < bzn. For precursor ions with 3 nitrile ligands, the tendency for direct

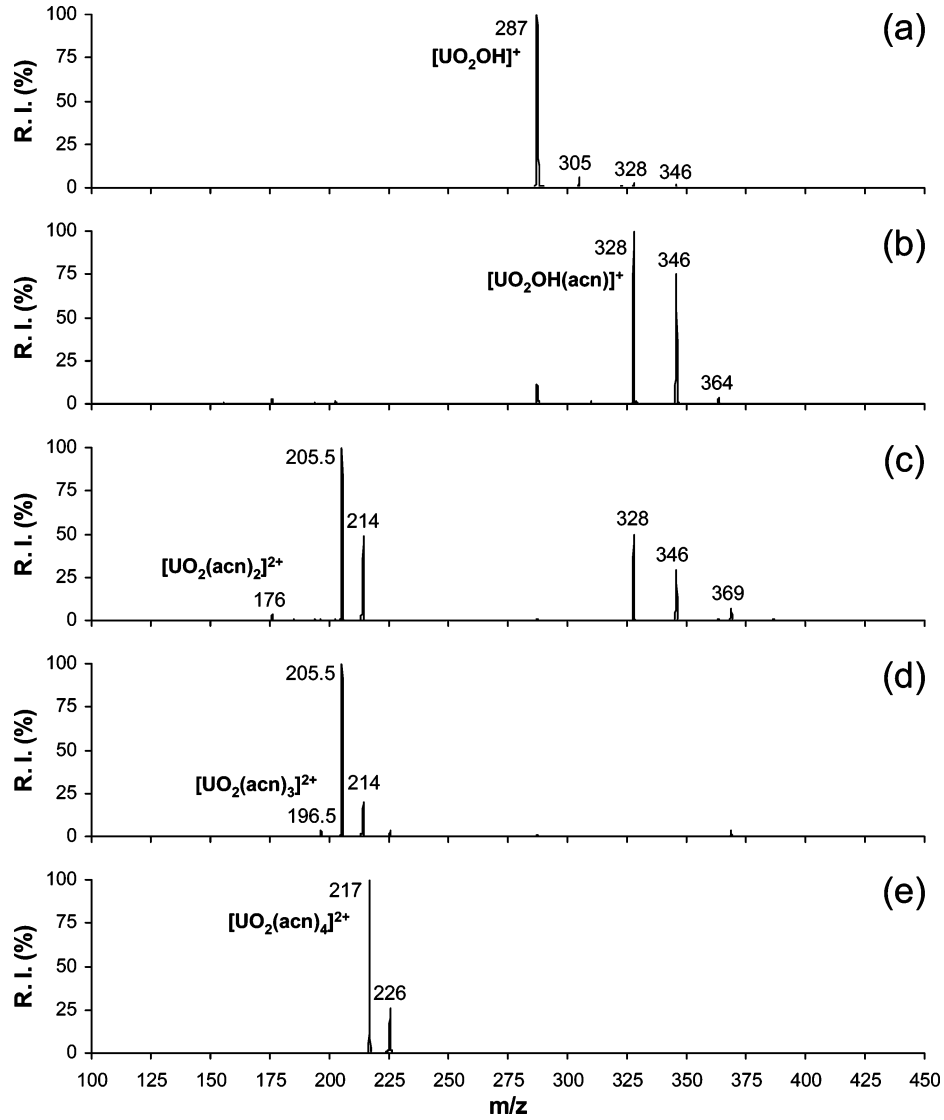

Figure 6. Product ion spectra generated by the isolation and collisional activation of doubly charged uranyl−acetonitrile complex ions: (a) $[UO_2(acn)_1]^{2+}$, (b) $[UO_2(acn)_2]^{2+}$, (c) $[UO_2(acn)_3]^{2+}$, (d) $[UO_2(acn)_4]^{2+}$, and (e) $[UO_2(acn)_5]^{2+}$. Applied activation voltages were in the range of 0.35−0.46 V, laboratory frame of reference.

addition of H_2O instead followed the trend pn > acn > bzn. This suggests that the increase in number of degrees of freedom for pn over acn assists hydration but that increasing basicity and/or steric hindrance for bzn over pn decreases the tendency for H_2O addition. The influence of increased nitrile ligand basicity, or more appropriately, donation of charge to the uranyl ion, is apparent in the decreased H_2O addition to the complexes with $n = 4$ progressing from acn to pn to bzn.

The charge reduction reactions exhibited by the doubly charged uranyl−nitrile complexes are consistent with those discussed previously for intracomplex transfer during the CID of H_2O complexes of divalent metal ions,[34] the unimolecular dissociation of $[Cu(H_2O)_n]^{2+}$,[35] the CID of $[Mg(C_3H_7OH)_n]^{2+}$,[36] and $[Mg(CH_3OH)_n]^{2+}$[37] and in reactions between H_2O and metal cluster cations.[38] For the propanol− and methanol−Mg^{2+} complexes in particular, the ultimate transfer of OH^- to the Mg ion involved bond breaking within a methanol ligand. In the present case, formation of the hydroxide involves transfer of OH^- to the uranyl−nitrile complexes from a neutral, gas-phase H_2O molecule.

In general, the gas-phase reactions of doubly charged metal ions and their complexes are dependent on the potential-energy curve for ligand addition and the relative positions of avoided crossings associated with curves for reactions that lead to possible charge-exchange products. In the present study, the potential charge exchange reactions include: (a) electron transfer from a gas-phase molecule (in this case H_2O or acn) to the uranyl complex ion and (b) transfer of OH^- from gas-phase H_2O to the uranyl complex ion. Similar reaction pathways and the relative positions of avoided crossings of potential energy curves have been discussed by Stace[39] and by Schröder and Schwarz[40] for systems such as gas-phase, hydrated Cu^{2+} and UF^{n+} cations. The results obtained here for the uranyl complexes with 1−3 nitrile ligands clearly show that a pathway involving electron-transfer alone, through collisions with the neutral species present in the He bath gas, is not competitive with one that includes the formal transfer of OH^-. The decreased tendency for charge transfer with increasing ligation within the precursor ion, as was observed for the uranyl complexes with 3−5 nitrile ligands, is consistent with earlier studies of mono- and hexahydrate metal ion complexes, in which the enthalpy change for hydrolysis (deprotonation of H_2O ligands) decreased as the degree of hydration within the complex ion increased.[41,42]

The intensity of the charge reduction products following isolation of UO_2^{2+} (generated when acn was used in the spray solvent) were relatively minor, which is surprising given the

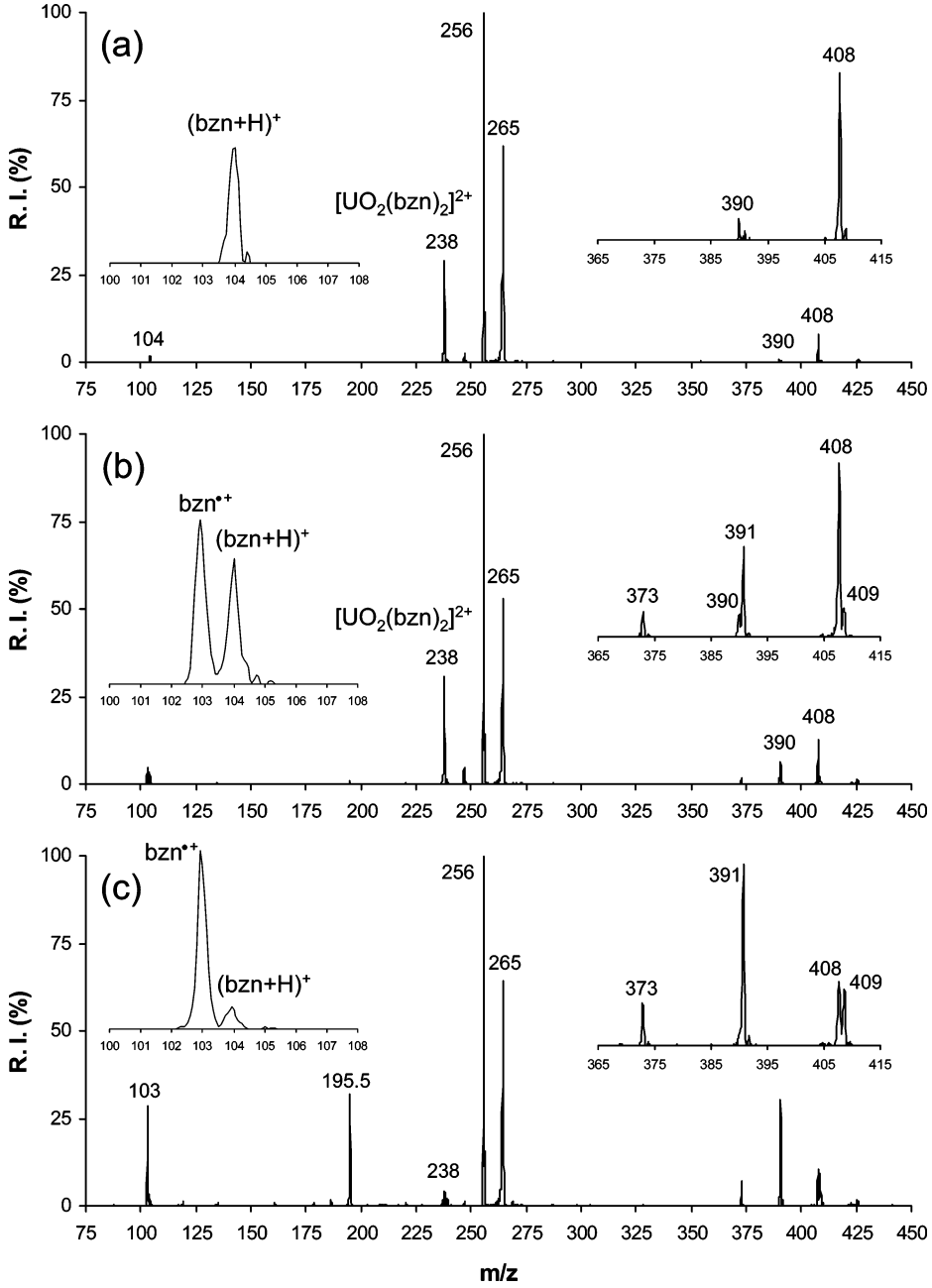

Figure 7. Product ion spectra generated by the isolation of $[UO_2(bzn)_2]^{2+}$: (a) 0 V applied activation voltage, (b) 0.5 V applied activation voltage, and (c) 0.73 V applied activation voltage. Applied voltages are in the laboratory frame of reference.

differences in magnitude between the ionization energy of UO_2^+ and H_2O, acn, or O_2. As noted earlier, the *m*/*z* ratios of the product ions generated following isolation and storage of the precursor ion at *m*/*z* 135 strongly support a composition assignment of UO_2^{2+}. We cannot completely eliminate the possibility of the presence of an isobaric contaminant ion. CID of the peak at *m*/*z* 135 produced the species at *m*/*z* 270 and 287, and no product ions at lower *m*/*z* ratios. This observation, combined with the argument presented above, supports the claim that the ion at *m*/*z* 135 is the uranyl ion.

The intensities of the charge reduction products at *m*/*z* 270 and 287, formed by the isolation of UO_2^{2+}, increased with extended isolation times (data not shown), which suggests that the rate for the reactions to product UO_2^+ and $[UO_2OH]^+$ are inherently slow. Comparison of the spectra shown in parts a and b of Figure 2 demonstrates a significant difference in the apparent rates of the charge exchange reactions for UO_2^{2+} and $[UO_2(acn)]^{2+}$ when the two precursor ions are exposed to comparable gas-phase environments. As discussed earlier, formation of the uranyl−hydroxide product ions involves the elimination of protonated nitrile ligands as shown in reaction 1, and a reaction channel involving simple electron transfer from an H_2O molecule to generate nitrile-ligated UO_2^+ was not observed. Transfer of OH^- as in (1) would be favored thermodynamically by the formation of the stable hydroxide and protonated nitrile and assisted by the fission of an activated complex containing two weakly bound cationic species. The nitrile ligand "receptor" liberated during the formation of the hydroxide in (1) is absent in the case of UO_2^{2+}, which lowers the probability for the charge reduction reaction.

CID of $[UO_2(RCN)_n]^{2+}$. The tendency for the uranyl−nitrile complex species to undergo charge reduction reactions to produce ligated $[UO_2OH]$ was also apparent during CID experiments. As shown in Figure 6a, CID of $[UO_2(acn)_1]^{2+}$ caused the formation of $[UO_2OH]^+$ and $[UO_2OH(acn)]^+$. The intensity of $[UO_2OH(acn)]^+$, when produced by CID of $[UO_2$-

$(acn)_1]^{2+}$, was greater than the intensity of the same ion when formed by the independent isolation and storage of $[UO_2OH]^+$. This observation supports the proposal that the ion at *m*/*z* 328 was formed as a direct CID product rather than as an acn adduct (formed by ion−molecule association reaction) to $[UO_2OH]^+$ after its formation from $[UO_2(acn)_1]^{2+}$. CID of $[UO_2(acn)_2]^{2+}$ at *m*/*z* 176 (Figure 6b) produced $[UO_2OH(acn)]^+$ and a hydrated adduct. Direct ligand elimination from $[UO_2(acn)_2]^{2+}$ to generate $[UO_2(acn)_1]^{2+}$ was not observed. CID of $[UO_2(acn)_3]^{2+}$ at *m*/*z* 196.5 (Figure 6c) generated three product ions: $[UO_2(acn)_2]^{2+}$ by the elimination of acn and the formation of $[UO_2OH(acn)]^+$ and $[UO_2OH(acn)_2]^+$. CID of $[UO_2(acn)_4]^{2+}$ and $[UO_2(acn)_5]^{2+}$ (parts d and e of Figure 6, respectively) demonstrated the elimination of a single acn ligand only.

In general, the CID of the pn versions of the complexes mirrored that of the acn complexes. Figure 7 shows three spectra collected for the $[UO_2(bzn)_2]^{2+}$ complex. In Figure 7a, the spectrum was produced by the isolation, without imposed collisional activation, of the species for 30 ms. The spectra in parts b and c of Figure 7 show the spectra that resulted from the CID of the same ion at activation amplitudes of 17 and 25%, respectively. As noted earlier, the charge reduction products observed following isolation of $[UO_2(bzn)_2]^{2+}$, without CID, included protonated bnz at *m*/*z* 104, $[UO_2OH(bzn)]^+$ at *m*/*z* 390, and $[UO_2OH(bzn)(H_2O)]^+$ at *m*/*z* 408. As is apparent in Figure 7b, inducing collisional activation of $[UO_2(bzn)_2]^{2+}$ lead to the appearance of four new product ions: the bzn radical ion at *m*/*z* 103 and ions at *m*/*z* 373, 391, and 409. The ion at *m*/*z* 373 corresponds in mass to the formation of $[UO_2(bzn)]^+$, presumably in a process that involved oxidation of a bzn ligand and reduction of the uranyl ion. Subsequent CID of the ion at *m*/*z* 373 caused the formation of UO_2^+ at *m*/*z* 270 via the elimination of 103 u, consistent with the composition assignment. The species at *m*/*z* 391 and 409 have masses consistent with formation of $[UO_2(bzn)(H_2O)]^+$ and $[UO_2(bzn)(H_2O)_2]^+$, respectively. Subsequent CID of the ions at *m*/*z* 391 and 409 (spectra not shown) showed the elimination of 18 u, consistent with the presence of H_2O ligands. At an activation amplitude of 25% (Figure 7c), the charge-exchange products resulting from electron transfer from bzn to the uranyl ion (i.e., *m*/*z* 103 and 373) and the hydrated forms of the products, and thus oxidation of a nitrile ligand, was higher than for reactions involving net hydroxide transfer from an H_2O collision partner. The appearance of the electron transfer products for the bzn complexes only is consistent with the significantly lower ionization energy of bzn relative to pn and acn.[27] The proposal that the direct oxidation of ligands during CID is a high-energy pathway is consistent with the dominant appearance of the charge reduction products involving formation of ligated $[UO_2OH]^+$ following isolation of the range of doubly charged uranyl−nitrile complexes and exposure to neutral H_2O in the ion trap. It is also evident that charge exchange reactions involving simple reduction of the doubly charged complexes by electron transfer (and oxidation of H_2O) is not a favored process for these precursor ions.

Conclusions

We have demonstrated here that ESI can be used to generate gas-phase, doubly charged complex cations containing the uranyl ion, UO_2^{2+}, and several nitrile ligands. For acn, doubly charged ions with between 0 and 5 coordinating, neutral ligands, were generated. For pn and bzn, complex cations with between 2 and 5 nitrile ligands were generated. In general, for species with 0−3 nitrile ligands, two general reaction pathways were observed: (a) formation of adducts through the addition of one or more H_2O or acn ligand and (b) charge reduction reactions that led to formation of ligated $[UO_2OH]^+$. For the bare uranyl ion, UO_2^{2+}, only the charge-exchange products UO_2^+ and UO_2OH^+, and hydrated versions of these species, were observed. For $[UO_2(acn)_1]^{2+}$, reactions with H_2O produced almost exclusively $[UO_2OH]^+$. For $[UO_2(RCN)_2]^{2+}$ and $[UO_2(RCN)_3]^{2+}$ complexes containing acn, pn, or bzn ligands, the principal charge reduction reaction observed involved elimination of a single nitrile ligand as a protonated species and addition of hydroxide, through reactions that involved collisions with neutral H_2O. For precursor complexes with 3 or 4 nitrile ligands, the direct H_2O addition was favored over the charge reduction reactions. Precursor complexes with 5 nitrile ligands were unreactive when isolated under similar conditions.

With respect to the complexity/size of the nitrile ligand, the trend for direct H_2O addition to the complex with 2 nitrile ligands, i.e., $[UO_2(RCN)_2]^{2+}$, was bzn > pn > acn. However, for complexes with 3 nitrile ligands, the trend for direct addition of H_2O was pn > acn > bzn, suggesting that the increase in number of degrees of freedom for pn over acn assists hydration but that increasing basicity and/or steric hindrance for bzn over pn decreases the tendency for H_2O addition. This proposal is supported by the low hydration tendency for the complex ion with 4 bzn ligands.

Comparison of the spectra generated by isolation and storage of the uranyl−benzonitrile complexes to spectra resulting from CID of the same species demonstrate that reaction pathways involving OH^- transfer are lower in energy than those involving direct oxidation of nitrile ligands, and pathways that involve reduction of precursor ion charge state via oxidation of neutral H_2O molecules.

Acknowledgment. MVS acknowledges support for this work by a grant from the National Science Foundation (CAREER-0239800), a First Award from the Kansas Technology Enterprise Corporation/Kansas NSF EPSCoR program, and a subcontract from the U.S. Department of Energy through the INEEL Institute. G.S.G. acknowledges support by the U.S. Department of Energy, Environmental Systems Research Program, under Contract DE-AC-07-99ID13727. Funds for the purchase of the LCQ-Deca instrument were provided by the Kansas NSF EPSCoR program and the Wichita State University College of Liberal Arts and Sciences.

References and Notes

(1) Gibson, J. K. *Int. J. Mass Spectrom. Ion Processes* **2002**, *213*, 1.
(2) Heinemann, C.; Cornehl, H. H.; Schwarz, H. *J. Organomet. Chem.* **1995**, *501*, 201−209.
(3) Gibson, J. K. *Organometallics* **1997**, *16*, 4214−4222.
(4) Gibson, J. K. *J. Am. Chem. Soc.* **1998**, *120*, 2633−2640.
(5) Gibson, J. K. *J. Mass Spectrom.* **1999**, *34*, 1166−1177.
(6) Gibson, J. K. *J. Vac. Sci. Technol. A-Vac. Surf. Films* **1997**, *15*, 2107−2118.
(7) Armentrout, P. B.; Beauchamp, J. L. *Chem. Phys.* **1980**, *50*, 27−36.
(8) Cornehl, H. H.; Heinemann, C.; Marcalo, J.; deMatos, A. P.; Schwarz, H. *Angew. Chem., Int. Edit. Engl.* **1996**, *35*, 891−894.
(9) Jackson, G. P.; King, F. L.; Goeringer, D. E.; Duckworth, D. C. *J. Phys. Chem. A* **2002**, *106*, 7788−7794.
(10) Gibson, J. K. *J. Mass Spectrom.* **2001**, *36*, 284−293.
(11) Van Stipdonk, M.; Anbalagan, V.; Chien, W.; Gresham, G. Groenewold, G.; Hanna, D. *J. Am. Soc. Mass Spectrom.* **2003**, *14*, 1205−1214.
(12) Van Stipdonk, M. J.; Chien, W.; Anbalagan, V.; Gresham, G.; Groenewold, G. S. *Int. J. Mass Spectrom.* **2004**, *237*, 175−183.
(13) Chien, W., Anbalagan, V.; Zandler, M.; Van Stipdonk, M.; Hanna, D.; Gresham, G.; Groenewold, G. *J. Am. Soc. Mass Spectrom.* **2004**, *15*, 777−783.

(14) Van Stipdonk, M. J.; Chien, W.; Anbalagan, V.; Bulleigh, K.; Hanna, D.; Groenewold, G. S. *J. Phys. Chem. A.* **2004**, *108*, 10448−10457.
(15) Gibson, J. K.; Haire, R. G.; Santos, M.; Marçalo, J.; Pires de Matos, A. *J. Phys. Chem. A.* **2005**, *109*, 2768−2781.
(16) Moulin, C.; Charron, N.; Plancque, G.; Virelizier, H. *Appl. Spectrosc.* **2000**, *54*, 843−848.
(17) Wu, Q. C., X.; Hofstadler, S. A.; Smith, R. D. *J. Mass Spectrom.* **1996**, *31*, 669−675.
(18) Dion, H. M.; Ackerman, L. K.; Hill, H. H. *Talanta* **2002**, *57*, 1161−1171.
(19) Dion, H. M. A., L. K.; Hill, H. H. *Int. J. Ion Mobil. Spectrom.* **2001**, *4*, 31−33.
(20) Pasilis, S. P. Pemberton, J. E. *Inorg. Chem.* **2003**, *42*, 6793−6800.
(21) Huan, H.; Chaudhary, S.; Van Horn, J. D. *Inorg. Chem.* **2005**, *44*, 813−815.
(22) Gresham, G. L.; Gianotto, A. K.; Harrington, P. de B.; Cao, L.; Scott, J. R.; Olson, J. E.; Appelhans, A. D.; Van Stipdonk, M. J.; Groenewold, G. S. *J. Phys. Chem. A* **2003**, *107*, 8530−8538.
(23) Wells, J. M.; Plass, W. R.; Patterson, G. E.; Ouyang, Z.; Badman, E. R.; Cooks, R. G. *Anal. Chem.* **1999**, *71*, 3405−3415.
(24) Li, H.; Plass, W. R.; Patterson, G. E.; Cooks, R. G. *J. Mass Spectrom.* **2002**, *37*, 1051−11058.
(25) Murphy III, J. P.; Yost, R. A. *Rapid Commun. Mass Spectrom.* **2000**, *14*, 270−273.
(26) McClellan, J. E.; Murphy III, J. P.; Mulholland, J. J.; Yost, R. A. *Anal. Chem.* **2002**, *74*, 402−412.
(27) Lias, S. G.; Bartmess, J. E.; Liebman, J. F.; Holmes, J. L.; Levin, R. D.; Mallard, W. G. Ion Energetics Data. In *NIST Chemistry WebBook, NIST Standard Reference Database Number 69*; Linstrom, P. J., Mallard, W. G., Eds.; National Institute of Standards and Technology, Gaithersburg MD, 20899; http://webbook.nist.gov.
(28) Burgess, J. *Metal Ions in Solution*; 1978; p 169.
(29) Fratiello, A.; Kubo, V.; Lee, R. E.; Schuster, R. E. *J. Phys. Chem.*, **1970**, *74*, 3726−3730.
(30) Bardin, N.; Rubini, P.; Madic, C. *Radiochim. Acta* **1998**, *83*, 189−194.
(31) Neuefeind, J.; Soderholm, L.; Skanthakumar, S. *J. Phys. Chem. A* **2004**, *108*, 2733−2739.
(32) Spencer, S.; Gagliardi, L.; Handy, N. C.; Ioannou, A. G.; Skylaris, C.-K.; Willets, A.; Simper, A. M. *J. Phys. Chem. A* **1999**, *103*, 1831−1837.
(33) Hanna, D.; Silva, M.; Morrison, J.; Tekarli, S.; Anbalagan, V.; Van Stipdonk, M. *J. Phys. Chem. A* **2003**, *107*, 5528−5537.
(34) Blades, A. T.; Jayaweera, P.; Ikonomou, M. G.; Kebarle, P. *J. Chem. Phys.* **1990**, *92*, 5900−5906.
(35) Stace, A. J.; Walker, N. R.; Firth, S. *J. Am. Chem. Soc.* **1997**, *119*, 10239−10240.
(36) Woodward, C. A.; Dobson, M. P.; Stace, A. J. *J. Phys. Chem.* **1996**, *100*, 5605−5607.
(37) Woodward, C. A.; Dobson, M. P.; Stace, A. J. *J. Phys. Chem. A.* **1997**, *101*, 2279−2287.
(38) Mikhailov, V. A.; Barran, P. E.; Stace, A. J. *Phys. Chem. Chem. Phys.* **1999**, *1*, 3461−3465.
(39) Stace, A. J. *J. Phys. Chem. A.* **2002**, *106*, 7993−8005.
(40) Schröder, D.; Schwarz, H. *J. Phys. Chem. A.* **1999**, *103*, 7385−7394.
(41) Chang, C. M.; Wang, M. K. *Chem. Phys. Lett.* **1998**, *286*, 46−48.
(42) George, P.; Glusker, J. P.; Trachtman, M.; Bock, C. W. *Chem. Phys. Lett.* **2002**, *351*, 454−456.